AIAA JOURNAL
Vol. 45, No. 2, February 2007

Simulation of a Moving Elastic Beam Using Hamilton's Weak Principle

Elliott J. Leigh* and Donald L. Kunz†
Air Force Institute of Technology, Wright–Patterson Air Force Base, Ohio 45433

DOI: 10.2514/1.25418

A proof-of-concept algorithm for calculating the general motion of elastic beams in the context of a multibody system analysis has been developed and validated. The governing equations for moving elastic beams with closed cross sections have been formulated using Hamilton's law of varying action. They are then discretized with a mixed space–time finite element scheme, which results in a system of nonlinear algebraic equations. These equations are solved using unconstrained optimization techniques, thereby obtaining steady-state and time-accurate solutions for linear and nonlinear structural dynamics problems. Solutions obtained for a variety of static, steady-state, and transient test cases have demonstrated the accuracy of the formulation. Illustrative examples, including the cantilever elastica problem, rotation of a beam at a constant angular velocity, and prescribed flapping motion of a beam, are presented.

Nomenclature

F_B	=	internal force
f_B	=	applied distributed force
H_B	=	angular momentum
H^{Bb}	=	rotation matrix
K_B	=	deformed curvature
k_b	=	undeformed curvature
M_B	=	internal moment
m	=	mass per unit length
m_B	=	applied distributed moment
P_B	=	momentum
u_b	=	displacement
V_B	=	deformed velocity
v_b	=	undeformed (prescribed) velocity
γ_B	=	force strain
δq	=	virtual displacement
$\delta\psi$	=	virtual rotation
κ_B	=	moment strain
$\rho_{B/b}$	=	rotation parameters
Ω_B	=	deformed angular velocity
ω_B	=	undeformed (prescribed) angular velocity

I. Introduction

MULTIBODY systems analysis (MSA) is an analytical tool used to solve problems of dynamics for complex mechanical systems. Many commercial and research software applications assemble the differential equations of motion for each component of the system and then append the algebraic constraint equations for each joint to these equations. This is known as the maximum coordinate set approach, and the resulting set of differential-algebraic equations (DAEs) is numerically stiff and must be solved with sophisticated algorithms. Although useful in many problems, this technique is not appropriate for certain aerospace applications that include flexible bodies undergoing large deformations and rotations. Some examples include helicopter rotor blades, highly flexible wings on aircraft, elastic linkages, satellites with flexible arms, and flapping wings.

A common criticism of DAE solvers is that they are "not sufficiently robust and may fail to produce a solution for some configurations" [1]. The purpose of this research is to explore an alternate approach to modeling and calculating the response of complex dynamic systems using Hamilton's weak principle (HWP) as the theoretical basis. This work is a proof of concept, in which the approach is applied to the structural dynamics of flexible beams. It may be extended directly to aircraft wings, rotor blades, robot arms, and structural members (spars, stringers, struts, etc.). Other authors have achieved measurable success in solving nonlinear initial value problems using HWP [2–4]. The use of the weak form serves as a mechanism for eliminating derivatives of field quantities, allowing for simpler shape functions in the analysis, while enforcing natural boundary conditions directly in the equations. It also provides a framework for developing a mixed finite element formulation of the problem.

An intrinsic equation for moving elastic beams was developed by Hodges [5]. This equation is derived from HWP and includes the full set of kinematic and constitutive equations, which are appended with Lagrange multipliers. Discretizing with mixed space–time finite elements transforms this complex, integral equation into a system of nonlinear algebraic equations that may be solved numerically. A similar approach for rigid bodies has been demonstrated successfully with some simple problems [4]. The difference is that flexible bodies require integration in both the space and time domains, resulting in a simultaneous boundary value problem in space and an initial value problem in time. The mixed formulation presented herein is unique in its inclusion of deformations, momenta, internal resultants, and generalized speeds and strains as independent field variables, which are evaluated simultaneously. The difference between this research and other space–time finite element models is that it avoids differential equation theory entirely. The full set of nonlinear algebraic equations for each time step are assembled and solved computationally, using the Gauss-Newton algorithm. To evaluate its robustness, this model has been tested against a variety of static, steady-state, and dynamic cantilever beam problems with known solutions.

II. Theory

The theoretical model of the moving beam is based on the nonlinear beam theory developed by Danielson and Hodges [6]. This model is applicable to long, slender beams with closed cross sections, unrestrained warping, and with initial curvature and twist. The beam and its properties are generalized along a one-dimensional reference line [5,7], as depicted in Fig. 1. In this manner, spatial integration of

Presented as Paper 1665 at the 47th AIAA/ASME/ASCE/AHS/ASC Structures, Structural Dynamics, and Materials Conference, Newport, Rhode Island, 1–4 May 2006; received 24 May 2006; revision received 29 August 2006; accepted for publication 29 August 2006.

*Captain, U.S. Air Force, 2950 Hobson Way. Member AIAA.
†Associate Professor, Department of Aeronautics and Astronautics, 2950 Hobson Way. Associate Fellow AIAA.

the domain is only required in one dimension. For thin beams with closed cross sections and moderate curvature, a separate 2-D cross-sectional analysis can be used to determine the constitutive properties [8]. The advantage of this approach is that the governing equations may be written for a beam of arbitrary cross-sectional properties along its length.

A rigorous treatment of the generalized kinematics and constitutive laws for beams is presented by Hodges [5]. An intrinsic formulation is desired, in which generalized speeds and strains are not written as functions of the displacements. There are many possible formulations based on the choice of generalized coordinates and rotation parameters [7]. For this paper, virtual displacements and rotations are used as generalized coordinates and Weiner–Milenkovic parameters are chosen for the rotation parameters [9]. This not only pushes the singularity to 2π, a value unlikely to be encountered in beam dynamics, but allows the rotation parameters to be easily rescaled long before reaching the singularity.

The exact, intrinsic equations for the moving beam are based on Hamilton's law of varying action.

$$\int_{t_1}^{t_2}(\delta L+\overline{\delta W})\,\mathrm{d}t-\sum_{k=1}^{n}\frac{\delta T}{\partial\dot{q}_k}\delta q_k\bigg|_{t_1}^{t_2}=0 \tag{1}$$

This equation can be expanded to include terms for kinetic energy, potential energy, and virtual work, then integrated in both the space and time domains. The kinematic and constitutive equations are appended with Lagrange multipliers. After extensive mathematical manipulation, this results in an exact, intrinsic equation for moving elastic beams [5,10].

$$\begin{aligned}
&\int_{t_1}^{t_2}\int_0^{\ell}\{(\dot{\overline{\delta q}}_B^T-\overline{\delta q}_B^T\tilde{\Omega}_B-\overline{\delta\psi}_B^T\tilde{V}_B)P_B+(\dot{\overline{\delta\psi}}_B^T-\overline{\delta\psi}_B^T\tilde{\Omega}_B)H_B\\
&\quad-[(\overline{\delta q}_B^T)'-\overline{\delta\psi}_B^T(\tilde{e}_1+\tilde{\gamma}_B)-\overline{\delta q}_B^T\tilde{K}_B]F_B-[(\overline{\delta\psi}_B^T)'\\
&\quad-\overline{\delta\psi}_B^T\tilde{K}_B]M_B+\delta V_B^T(P_B-mV_B+m\tilde{\tilde{\xi}}_B\Omega_B)+\delta\Omega_B^T(H_B-I\Omega_B\\
&\quad-m\tilde{\tilde{\xi}}_BV_B)+\delta\gamma_B^T(A\gamma_B+B\kappa_B-F_B)+\delta K_B^T(B^T\gamma_B+D\kappa_B\\
&\quad-M_B)+\overline{\delta P}^T(v_b+\tilde{w}_bu_b-C^{bB}V_B)+\overline{\delta F}^T[C^{bB}(\gamma_B+e_1)\\
&\quad-(e_1+\tilde{k}_bu_b)]+\overline{\delta H}^T(H^{Bb})^{-1}(C^{Bb}w_b-\Omega_B)\\
&\quad+\overline{\delta M}^T(H^{Bb})^{-1}(K_B-C^{Bb}k_b)-\dot{\overline{\delta P}}^Tu_b+(\overline{\delta F}^T)'u_b-\dot{\overline{\delta H}}^T\rho_{B/b}\\
&\quad+(\overline{\delta M}^T)'\rho_{B/b}-\delta U_G+\overline{\delta W}\}\,\mathrm{d}x_1\,\mathrm{d}t\\
&\quad+\int_{t_1}^{t_2}(\overline{\delta q}_B^t\hat{F}_B+\overline{\delta\psi}_B^t\hat{M}_B-\overline{\delta F}^t\hat{u}_b-\overline{\delta M}^t\hat{\rho}_{B/b})|_0^{\ell}\,\mathrm{d}t\\
&\quad+\int_0^{\ell}(\overline{\delta P}^T\hat{u}_b+\overline{\delta H}^T\hat{\rho}_{B/b}-\overline{\delta q}_B^T\hat{P}_B-\overline{\delta\psi}_B^T\hat{H}_B)|_{t_1}^{t_2}\,\mathrm{d}x_1=0
\end{aligned} \tag{2}$$

To use this equation to obtain time-accurate simulations of moving beam problems, a space–time finite element discretization is used. Space–time finite element techniques are common in the literature for beam and rod applications [11–14]. The approach used herein introduces a mixed formulation in which all field quantities are solved simultaneously. Integration is performed with shape functions of the lowest possible order. In this case, bilinear shape functions are used for the variational quantities $\overline{\delta q}_B$ and $\overline{\delta\psi}_B$, and linear shape functions are used for $\overline{\delta P}$, $\overline{\delta H}$, δV_B, $\delta\Omega_B$, $\overline{\delta F}$, $\overline{\delta M}$, $\delta\gamma_B$, and δK_B. For all nonvariational quantities, constant shape functions are used [10].

Substituting the shape functions and performing the integration results in a system of 20 nonlinear algebraic equations [10]. Only 18 of these equations are independent and, therefore, two are eliminated. Four additional equations and unknowns may also be removed through algebraic manipulation. A final set of 14 equations and 14 unknowns remains.

$$\begin{aligned}
&\frac{\Delta x}{4}\left(\hat{P}_1-\hat{P}_2\right)-\frac{\Delta x\Delta t}{8}\left[\tilde{\tilde{\Omega}}_B\left(\hat{P}_1+\hat{P}_2\right)-\tilde{\tilde{K}}_B\left(\hat{F}_1+\hat{F}_2\right)\right]\\
&\quad+\frac{\Delta t}{4}\left(\hat{F}_2-\hat{F}_1\right)+\frac{\Delta x\Delta t}{4}(f_B+mg_B)=0
\end{aligned} \tag{3}$$

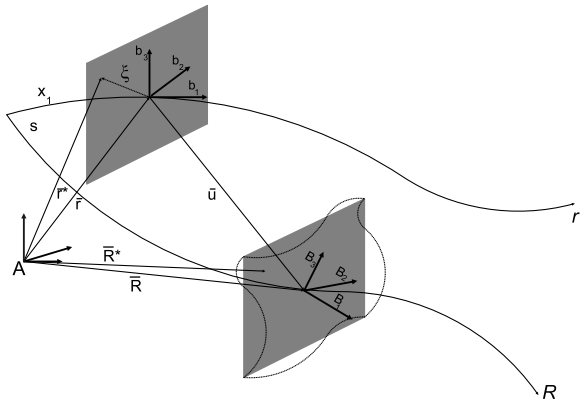

Fig. 1 Geometry of the undeformed *b* and deformed *B* beams. In the *b* basis, b_1 is parallel to the beam's reference line. In the *B* basis, B_1 is normal to the cross section, but may not be parallel to the reference line if warping is present. The vector *u* is the displacement of the section, and a direction cosine matrix C^{Bb} describes the deformation due to bending and twist. The *A* basis represents a frame in which motion is known in the inertial frame and is treated as the inertial frame in this paper.

$$\begin{aligned}
&\frac{\Delta x\Delta t}{8}\left[-\tilde{\bar{V}}_B\left(\hat{P}_1+\hat{P}_2\right)-\tilde{\tilde{\Omega}}_B\left(\hat{H}_1+\hat{H}_2\right)+\left(\tilde{e}_1+\tilde{\tilde{\gamma}}_B\right)\left(\hat{F}_1\right.\right.\\
&\quad\left.\left.+\hat{F}_2\right)+\tilde{\tilde{K}}_B\left(\hat{M}_1+\hat{M}_2\right)\right]+\frac{\Delta x}{4}\left(\hat{H}_1-\hat{H}_2\right)\\
&\quad+\frac{\Delta t}{4}\left(\hat{M}_2-\hat{M}_1\right)+\frac{\Delta x\Delta t}{4}\left(m_B+\tilde{\tilde{\xi}}_Bmg_B\right)=0
\end{aligned} \tag{4}$$

$$\tfrac{1}{2}\left(\hat{P}_1+\hat{P}_2\right)-m\bar{V}_B+m\tilde{\tilde{\xi}}_B\bar{\Omega}_B=0 \tag{5}$$

$$\tfrac{1}{2}\left(\hat{H}_1+\hat{H}_2\right)-I\bar{\Omega}_B-m\tilde{\tilde{\xi}}_B\bar{V}_B=0 \tag{6}$$

$$A\bar{\gamma}_B+B\left(\bar{K}_B-k_b\right)-\tfrac{1}{2}\left(\hat{F}_1+\hat{F}_2\right)=0 \tag{7}$$

$$B^T\bar{\gamma}_B+D\left(\bar{K}_B-k_b\right)-\tfrac{1}{2}\left(\hat{M}_1+\hat{M}_2\right)=0 \tag{8}$$

$$\frac{\Delta t}{2}(v_b+\tilde{\omega}_b\bar{u}_b-C^{bB}\bar{V}_B)+\bar{u}_b-\hat{u}_1=0 \tag{9}$$

$$\frac{\Delta t}{2}(v_b+\tilde{\omega}_b\bar{u}_b-C^{bB}\bar{V}_B)+\hat{u}_3-\bar{u}_b=0 \tag{10}$$

$$\frac{\Delta t}{2}(H^{Bb})^{-1}(C^{Bb}\omega_b-\bar{\Omega}_B)+\bar{\rho}_{B/b}-\hat{\rho}_1=0 \tag{11}$$

$$\frac{\Delta t}{2}(H^{Bb})^{-1}(C^{Bb}\omega_b-\bar{\Omega}_B)+\hat{\rho}_3-\bar{\rho}_{B/b}=0 \tag{12}$$

$$\frac{\Delta x}{2}[C^{bB}(\bar{\gamma}_B+e_1)-(e_1+\tilde{k}_b\bar{u}_b)]+\hat{u}_4-\bar{u}_b=0 \tag{13}$$

$$\frac{\Delta x}{2}[C^{bB}(\bar{\gamma}_B+e_1)-(e_1+\tilde{k}_b\bar{u}_b)]+\bar{u}_b-\hat{u}_2=0 \tag{14}$$

$$\frac{\Delta x}{2}(H^{Bb})^{-1}(\bar{K}_B-C^{Bb}k_b)+\hat{\rho}_4-\bar{\rho}_{B/b}=0 \tag{15}$$

$$\frac{\Delta x}{2}(H^{Bb})^{-1}(\bar{K}_B-C^{Bb}k_b)+\bar{\rho}_{B/b}-\hat{\rho}_2=0 \tag{16}$$

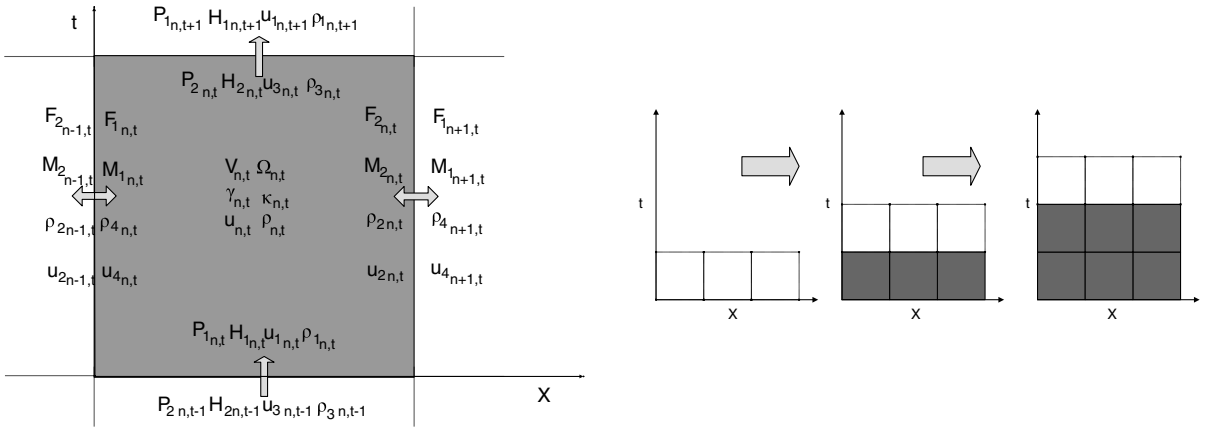

a) Space–time finite element **b) Time marching procedure**

Fig. 2 The space–time finite element depicted in Fig. 2a shares values of force, moment, displacement, and rotation at its spatial edges with the adjacent elements. The temporal edges of the element are used to generate initial conditions for momenta and displacements for the following time step. This allows for a solution procedure in which all elements are evaluated simultaneously within each time interval, and the algorithm marches forward in time, as illustrated in Fig. 2b.

This system of nonlinear algebraic equations satisfies the constitutive laws (5–8), kinematics (9–16), and equilibrium conditions (3) and (4) for a single beam element over a finite time interval. Figure 2a depicts the space–time finite element for which these equations are derived. This element is unlike traditional displacement formulation elements for which deformations are defined at the nodes. Here, quantities are defined along the space and time edges (due to boundary conditions introduced with HWP) and are considered to be constant within the element. Solving this system of equations allows forces, momenta, strains, velocities, and displacements to be solved simultaneously (a mixed formulation), and enforces natural boundary conditions explicitly in the equations.

The beam is discretized into N_x elements along its reference line and solved over a time interval of N_t increments. There are $22N_x$ field quantities and $14N_x$ equations in each time interval. For each time step there are $4N_x$ initial conditions and 4 boundary conditions. Boundary conditions come from $\hat{\rho}_2$, $\hat{\rho}_4$, $\hat{u}_2$, $\hat{u}_4$, $\hat{F}_1$, $\hat{F}_2$, $\hat{M}_1$, or $\hat{M}_2$, depending on the problem. For a cantilevered beam, the root displacements are fixed and the tip forces and moments are prescribed. The beam elements also share $4(N_x - 1)$ boundary values with adjacent elements [Fig. 2a]. For a continuous beam, the values of q_b, $\rho_{B/b}$, F_B, and M_B are shared. For various types of joints (such as a hinge), some of these quantities will be shared and others may be prescribed. Applying these initial and boundary conditions reduces the problem to a system of $14N_x$ equations and $14N_x$ unknowns at each time step. After the solution at one time step is obtained, the initial conditions for the next time step are available. This formulation is well-suited for a time marching algorithm [Fig. 2b], and is typical of other space–time finite element formulations in the literature [11–13], in which an initial value problem in time and boundary value problem in space are solved simultaneously.

Many numerical procedures are available to solve systems of nonlinear algebraic equations. In this paper, a Gauss-Newton method is used. The complete set of $14N_x$ equations is assembled in the following form:

$$\boldsymbol{F}(\boldsymbol{x}) = 0 \tag{17}$$

where Eq. (17) is a vector equation. Equation (17) is solved as an unconstrained optimization problem in which the residuals of F are minimized to yield the solution. Often, the convergence of the problem depends on how close the initial guess is to the solution and, in some cases, a poor initial guess will either prevent the algorithm from converging or cause it to converge to a minimum that is not the correct solution. In many dynamic problems, the solution from the previous time step can be used as the initial guess for the next time step. Generally, a vector of zeros can be used as the initial guess for steady-state problems. These techniques work well for steady-state problems with small displacements and for dynamic problems in which the time step is sufficiently small. To improve the initial guess for dynamic problems, numerical derivatives can be used from the sequence of previous solutions to obtain a better guess [10]. For static problems with large displacements, the problem can be solved incrementally. First, the applied load is divided into increments and then solved at the smallest increment, using an initial guess of zero. The solution is then used as the initial guess for the next load increment. The algorithm continues in this manner until reaching the final loading condition, which yields the final solution. With this technique, the solution for each increment is close to the solution from the previous increment, improving convergence.

Numerical algorithms of this type may also perform poorly when the magnitudes of the variables are poorly scaled, and may fail to converge to any solution [15]. For the beam problem, units of force are generally very large and units of displacement are small, resulting in a poorly scaled state vector. One means for rescaling the variables is to change the units, which then rescales the state vector $\boldsymbol{x}$. Although this approach was successful for every class of problem investigated herein, a more generally applicable approach using nondimensional parameters would be preferred.

III. Results

The mixed space–time formulation for a moving beam described previously was validated using a variety of cantilever beam problems for which the solutions were known [10]. Static cases included the axial loading of a uniform rod with concentrated and distributed forces, torsional loading of both uniform and tapered rods with concentrated and distributed moments, transverse loading of a uniform Timoshenko beam with concentrated and distributed forces and moments, the cantilevered elastica problem, and a uniform beam subject to a static follower force. Steady-state problems included a uniform beam rotating at a constant angular velocity and a uniform

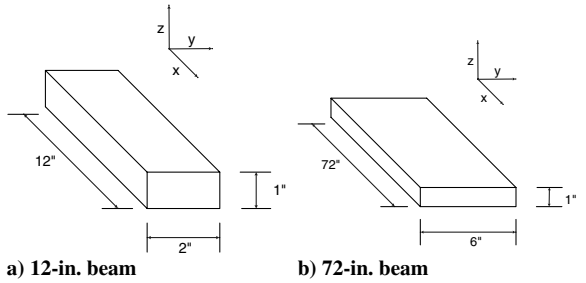

a) 12-in. beam **b) 72-in. beam**

Fig. 3 Depiction of the various geometries used in simulations.

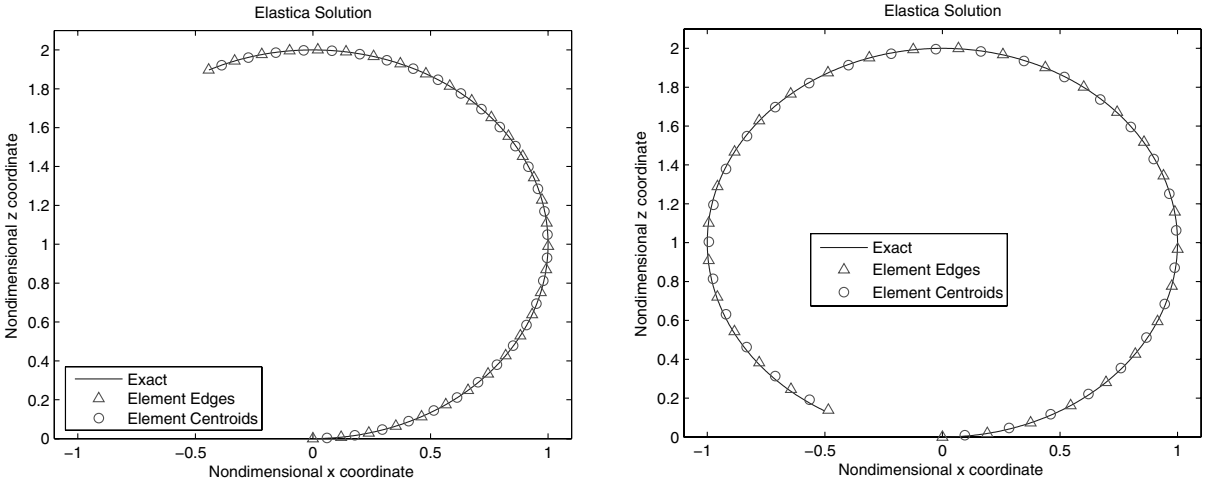

a) 500 in.·lb tip moment **b) 800 in.·lb tip moment**

Fig. 4 Cantilevered elastica results for a tip moment.

beam rotating at a constant angular velocity with an applied transverse distributed load. Dynamic problems included axial and torsional vibration of a uniform rod, transverse vibration of a uniform beam, prescribed spin-up of a uniform beam, and prescribed flapping motion of a uniform beam. Calculated solutions for all cases yielded excellent results compared with the known solutions. Because space does not permit all cases to be presented herein, a representative sample of the most interesting cases are discussed next.

Static problems were solved over a single time interval for which the initial and final displacements and momenta were constrained to be equal. The cantilevered elastica was used to test this methodology for a highly nonlinear static problem. Elastica is the shape of the elastic curve that comes from solving the differential equation for a beam with large deflections [16].

$$\frac{M}{EI} = \frac{\partial^2 v/\partial x^2}{[1 + (\partial v/\partial x)^2]^{3/2}} \tag{18}$$

A 12-in. cantilevered beam [Fig. 3a] with $E = 10^4$ psi, $\nu = 0.35$, and $\rho = 0.098$ $\text{lb}_m/\text{in.}^3$ was loaded with a bending moment at the tip about the y axis. Results for two different loading conditions and 30 beam elements are displayed in Fig. 4, in which the deformed coordinates are nondimensionalized by the radius of curvature. To evaluate convergence, the x–z coordinates of the solution are compared with those of the exact solution [Eq. (18)] and the mean error is determined. Figure 5 illustrates the convergence of the solutions. In the most extreme case, the mean error in $\bar{u}$ is less than 1% when 40 beam elements are used. Although the scenario of curling a beam into a circle does not directly apply to the loading of a wing or rotor blade, it does demonstrate the accuracy of this solution methodology for an exaggerated case and demonstrates the algorithm's ability to handle highly nonlinear problems.

Steady-state problems were solved in a manner similar to the static problems. One of the steady-state problems that was solved involves the steady, flatwise rotation of a cantilevered beam. The velocities v_b and ω_b are specified for each element to generate a beam that is rotating at a constant velocity about its root, with fixed-free boundary

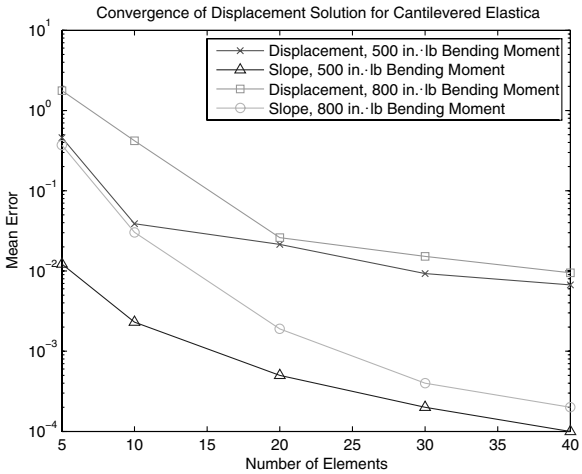

Fig. 5 Mean error vs number of elements for the cantilevered elastica.

conditions. In this configuration, the beam will experience elongation due to the inertial forces that hold it in place. The exact solution to this problem comes from the following transcendental equations [10].

$$F(x) = \int_x^\ell [r(x) + u(x)]\omega^2 m \, \mathrm{d}x \tag{19}$$

$$u(x) = \frac{1}{AE}\int_0^x F(x) \, \mathrm{d}x \tag{20}$$

Using a rigid-body approximation to estimate the internal force, the following equations are obtained.

$$F(x) \approx \tfrac{1}{2} m\omega^2(\ell^2 - x^2) \tag{21}$$

$$u(x) \approx \frac{1}{AE}\int_0^x \left[\frac{1}{2} m\omega^2(\ell^2 - x^2)\right] \mathrm{d}x \tag{22}$$

Table 1 Summary of convergence for steady rotation problems

Configuration		Mean difference from previous mesh						
Geometry	Speed	2	3	5	7	10	20	30
12-in.	3 Hz	0.5000	0.0758	0.0355	0.0113	0.0058	0.0029	0.0007
	20 Hz	0.5101	0.0773	0.0363	0.0115	0.0060	0.0030	0.0007
12-in. elastic	3 Hz	0.5002	0.0762	0.0357	0.0113	0.0059	0.0029	0.0007
	20 Hz	0.6254	0.0946	0.0451	0.0139	0.0072	0.0039	0.0009
72-in.	3 Hz	0.5000	0.0758	0.0355	0.0113	0.0058	0.0029	0.0007
	20 Hz	0.5004	0.0759	0.0355	0.0113	0.0058	0.0029	0.0007

These equations are adequate for beams made of stiff materials such as aluminum, for which the deformations are small. However, for highly elastic materials, they are not sufficient. Several cases were investigated for this problem, using various material properties and geometries at both 3 and 20 Hz [10]. The first beam uses the geometry of the 12-in. beam from Fig. 3a and a Young's modulus of $E = 10^7$ psi for aluminum. The second beam is also made of aluminum and uses the geometry of the 72-in. beam in Fig. 3b. For the final beam, the Young's modulus for the 12-in. beam geometry is decreased to $E = 10^3$ psi, resulting in significantly larger deformations, particularly at 20 Hz. Table 1 shows the percent change for each of the seven meshes used for each scenario. At 30 elements, the percent change in displacement from 20 elements has decreased to less than 1%, and the solution is seen to be converged.

This problem was the first in which scaling difficulties were encountered. Solutions for long beams, large meshes, and high velocities were unattainable when standard units of pounds, inches, and seconds were used. Successful convergence was finally achieved when the basic unit of time was changed to milliseconds. The exception to this occurred for the 12-in. elastic beam at 3 Hz with 10 or more elements. It was necessary in those cases to switch back to standard units to obtain the correct solution. Clearly, a formulation that uses nondimensional parameters will be more successful at overcoming this problem.

Figure 6 shows the progression of the solution as the number of elements is increased for the 12-in. highly elastic beam. The rigid-body approximation is also displayed and appears to work well while displacements are relatively small. However, this approximation fails at high speed, while the model continues to converge toward a more accurate solution. This is an excellent example of an application for this type of solver, when modeling the system using a rigid-body approximation yields an invalid solution.

To simulate a flapping wing, a cantilevered beam is discretized into 10 spatial elements and given a periodic angular velocity about the y axis, causing it to flap at 2 Hz and reach a maximum amplitude of 30 deg above and below the horizon. The oscillation is forced by prescribing the values for ω_b, as follows (t is in milliseconds):

$$\omega_b(t) = \frac{\pi^2}{1500}\cos\left(\frac{\pi}{250}t\right) \tag{23}$$

The simulation is performed with the 12-in. beam from Fig. 3a using Young's moduli of both $E = 10^4$ psi and $E = 10^7$ psi. The z coordinate of the tip is recorded in the inertial frame for each beam to depict the flapping motion (see Fig. 7). Excitation of the fundamental flapping frequency is observed in the displacement of the tip over time. The frequency of this vibration is obtained through a fast Fourier transform (FFT) of the time data [10]. The exact solution for the frequency is determined from the following equation [17].

$$\omega_n = 3.516\sqrt{EI/mL^3} \tag{24}$$

Using a Δt of 0.2 ms and 10,000 time steps provides 2 s of data, which yields four cycles of the flapping motion and a sufficient number of data points to accurately capture the fundamental frequency of vibration for each beam. The frequency response for each case is illustrated in Fig. 8.

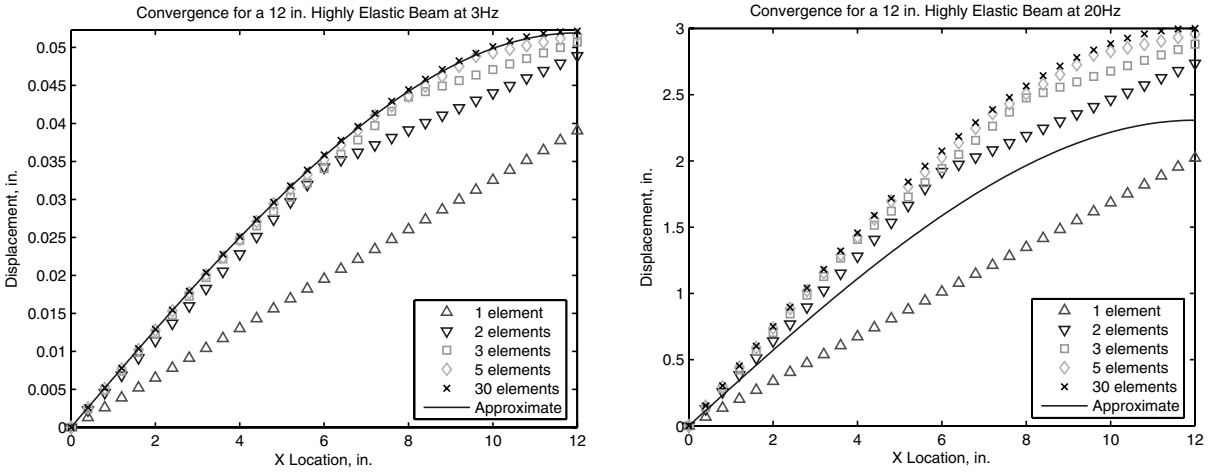

a) 12-in. elastic 20 Hz **b) 12-in. elastic 3 Hz**

Fig. 6 Displacement solutions for various mesh sizes of a steady, rotating elastic beam.

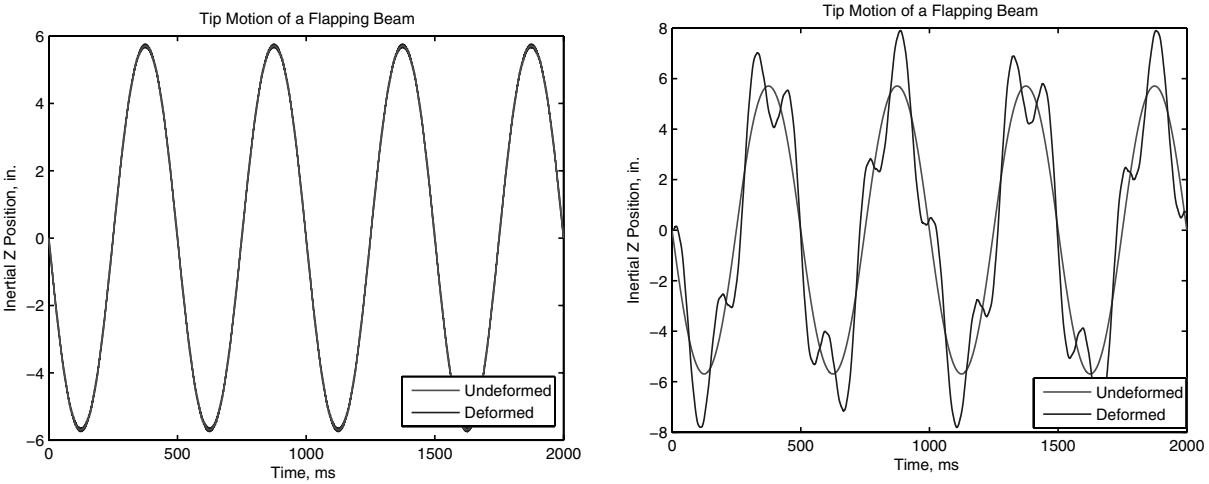

a) Aluminium beam; *E*=10*e*6 psi **b) Highly elastic beam; *E*=10*e*3 psi**

Fig. 7 Inertial tip response in the flapping maneuver for a 12-in beam; $\Delta t = 0.2$ ms and $N_x = 10$.

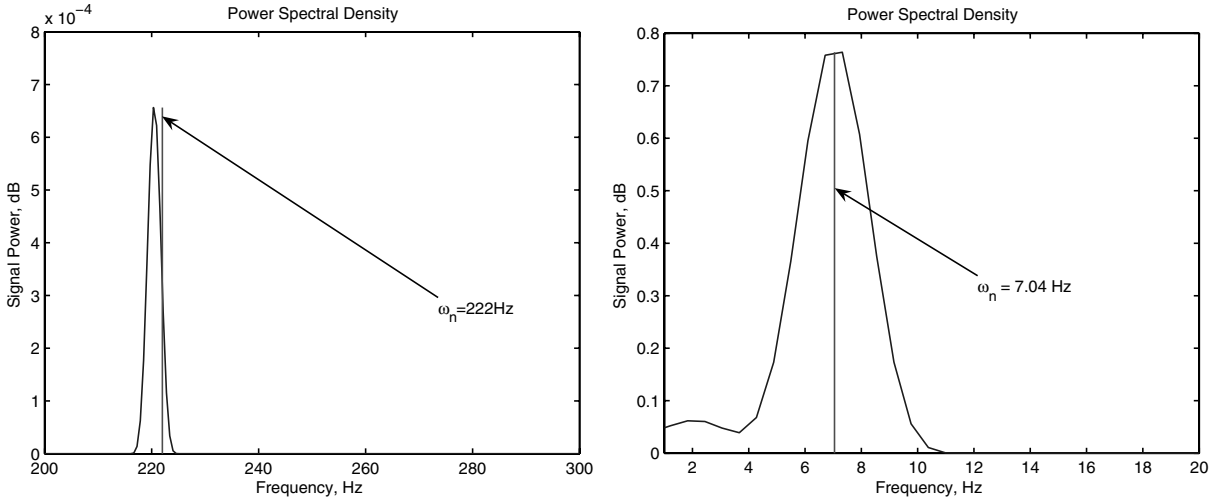

a) Aluminium beam; E=10e6 psi **b) Highly elastic beam; E=10e3 psi**

Fig. 8 Frequency response of the flapping maneuver for a 12-in beam; $\Delta t = 0.2$ ms and $N_x = 10$s.

The frequency responses of both beams indicate oscillation at their respective natural frequencies, with the elastic beam experiencing much larger deformations. Figure 7 best illustrates the response of the tip, showing both the forced oscillation at 2 Hz and the actual position of the tip that includes the deformation. The aluminum beam experiences very small deformations, whereas the elastic beam has significant deformation in addition to the prescribed motion.

IV. Conclusions

This research has successfully applied HWP to the development of a multibody dynamics formulation for flexible bodies. After deriving Hamilton's law for beams with closed cross sections (a technique that has been established in the literature [5]), a mixed space–time finite element discretization was performed to generate a system of nonlinear algebraic equations. These equations were solved numerically for common problems in engineering mechanics and structural dynamics. The discretization scheme and solution algorithm provide an alternative to existing multibody dynamics programs by avoiding the solution of differential-algebraic equations altogether and using optimization techniques to satisfy the system of nonlinear algebraic equations at each time step. This method is applicable to a wide class of problems; accurate results were obtained for a variety of scenarios, including static equilibrium, steady-state motion, vibrations, and dynamic response.

The intent of this research is to serve as a proof of concept for the application of HWP to flexible body multibody dynamics. Although many types of problems were investigated, the formulation is designed to handle much more. Further applications will be able to successfully obtain solutions to problems of initially curved and twisted beams, variable geometries, and orthotropic and anisotropic materials. The use of alternate boundary and joint conditions between elements will make this formulation more useful for multibody programs. Extending the principles used to other types of elements (shells, plates, membranes, etc.) is ultimately necessary to investigate the full application of HWP in elastodynamics. This will require a separate development using the unique constitutive, kinematic, and energy relationships for these types of bodies. An architecture for a software code using this application will require an element library and an efficient method for assembling the state vector, which involves complex boundary conditions associated with connections between different element types. The research presented herein is a first step in this direction.

Acknowledgment

The authors wish to acknowledge the assistance of Dewey H. Hodges, who provided valuable insights into the implementation of Hamilton's weak principle and space–time finite element techniques.

References

[1] Kunz, D. L., "Multibody System Analysis Based on Hamilton's Weak Principle," *AIAA Journal*, Vol. 39, No. 12, Dec. 2001, pp. 2382–2388.

[2] Peters, D. A., and Izadpanah, A. P., "HP-Version Finite Elements for the Space Time Domain," *Computational Mechanics*, Vol. 3, No. 2, 1988, pp. 73–88.

[3] Hodges, D. H., and Bless, R. R., "Weak Hamiltonian Finite Element Method for Optimal Control Problems," *Journal of Guidance, Control, and Dynamics*, Vol. 14, No. 1, 1991, pp. 148–155.

[4] Kunz, D. L., "Implementation of a Generalized Multibody Approach for Analysis of Dynamic Systems," AIAA Paper 2005-2348, 2005.

[5] Hodges, D. H., "A Mixed Variational Formulation Based on Exact Intrinsic Equations for Dynamics of Moving Beams," *International Journal of Solids and Structures*, Vol. 14, No. 11, Nov. 1990, pp. 1253–1273.

[6] Danielson, D. A., and Hodges, D. H., "Nonlinear Beam Kinematics by Decomposition of the Rotation Tensor," *Journal of Applied Mechanics*, Vol. 54, June 1987, pp. 258–262.

[7] Hodges, D. H., "Geometrically Exact, Intrinsic Theory for Dynamics of Curved and Twisted Anisotropic Beams," *AIAA Journal*, Vol. 41, No. 6, June 2003, pp. 1131–1137.

[8] Atilgan, A. R., and Hodges, D. H., "A Geometrically Nonlinear Analysis for Nonhomogeneous, Anisotropic Beams," *Proceedings of the 30th Structures, Structural Dynamics and Materials Conference*, Part 2B, AIAA, Washington, D.C., 1989, pp. 895–908.

[9] Bauchau, O. A., and Trainelli, L., "The Vectorial Parameterization of Rotation," *Nonlinear Dynamics*, Vol. 32, No. 1, Apr. 2003, pp. 71–92.

[10] Leigh, E. J., "Simulation of a Moving, Elastic Beam Using Hamilton's Weak Principle," M.S. Thesis, Air Force Institute of Technology, Wright–Patterson AFB, OH, Mar. 2006.

[11] Grohmann, B. A., Wallmersperger, T., and Kroplin, B.-H., "Time-Discontinuous Stabilized Space-Time Finite Elements for Timoshenko Beams," *AIAA Journal*, Vol. 39, No. 11, Nov.2001, pp. 2158–2166.

[12] Atilgan, A. R., and Hodges, D. H., "Space-Time Mixed Finite Elements for Rods," *Journal of Sound and Vibration*, Vol. 192, No. 3, 1996, pp. 731–739.

[13] Hughes, T. J. R., and Hulbert, G. M., "Space-Time Finite Element Methods for Elastodynamics: Formulations and Error Estimates," *Computer Methods in Applied Mechanics and Engineering*, Vol. 66, No. 3, Feb. 1988, pp. 339–363.

[14] Hou, L. J., and Peters, D. A., "Application of Triangular Space-Time Finite Elements to Problems of Wave Propagation," *Journal of Sound and Vibration*, Vol. 173, No. 5, 1994, pp. 611–632.

[15] Dennis, J. E., and Schnabel, R. B., *Numerical Methods for Unconstrained Optimization and Nonlinear Equations*, Society for Industrial and Applied Mathematics, Philadelphia, 1996.

[16] Hibbeler, R. C., *Mechanics of Materials*, 4th ed., Prentice–Hall, Upper Saddle River, NJ, 2000.

[17] Cook, R. D., Malkus, D. S., Plesha, M. E., and Witt, R. J., *Concepts and Applications of Finite Element Analysis*, 4th ed., Wiley, New York, 1974.

A. Berman
Associate Editor